

RELATIVISTIC EFFECTS IN ELECTRON SCATTERING: THE CASE OF THE TRANSVERSE-LONGITUDINAL RESPONSE AND LEFT-RIGHT ASYMMETRY

J.M. UDIAS^{1,A}, J.A. CABALLERO^{1,B}, E. MOYA DE GUERRA¹, J.E. AMARO² and T.W. DONNELLY³

¹*Instituto de Estructura de la Materia, CSIC Serrano 123, E-28006 Madrid, Spain*

^a*Departamento de Física Atómica, Molecular y Nuclear, Universidad Complutense de Madrid, E-28040 Madrid, Spain*

^b*Departamento de Física Atómica, Molecular y Nuclear, Universidad de Sevilla, Apdo. 1065, E-41080 Sevilla, Spain*

²*Departamento de Física Moderna, Universidad de Granada, E-18071 Granada, Spain*

³*Center for Theoretical Physics, Laboratory for Nuclear Science and Department of Physics, Massachusetts Institute of Technology, Cambridge, MA 02139 USA*

Predictions for electron induced proton knockout from $p_{1/2}$ and $p_{3/2}$ shells in ^{16}O are presented using various approximations for the relativistic nucleonic current. Results for differential cross section, transverse-longitudinal response (R_{TL}) and left-right asymmetry A_{TL} are compared at $|Q^2| = 0.8$ (GeV/c)². We show that there are important dynamical and kinematical relativistic effects which can be tested by experiment.

Most theoretical work on $(e, e'p)$ has been carried out on the basis of non-relativistic approximations to the nucleon current, namely the standard distorted wave impulse approximation (DWIA) ¹. Data analyses based on DWIA have met two major difficulties: a) The spectroscopic factors extracted from low- p_m data are too small compared with theoretical predictions. b) DWIA calculations compatible with the low- p_m data predict much smaller cross sections at high- p_m than those experimentally observed ². Although short-range correlations are expected to increase the high-momentum components, their effect is negligible ³ at the small missing energies of these high- p_m data.

In recent years the relativistic mean-field approximation has been successfully used for the analyses of both low- p_m ^{4,5,6} and high- p_m ⁷ data. In the relativistic distorted-wave impulse approximation (RDWIA), the nucleon current

$$J_N^\mu(\omega, \vec{q}) = \int d\vec{p} \bar{\psi}_F(\vec{p} + \vec{q}) \hat{J}_N^\mu(\omega, \vec{q}) \psi_B(\vec{p}) \quad (1)$$

is calculated with relativistic ψ_B and ψ_F wave functions for initial bound and final outgoing nucleons, respectively. \hat{J}_N^μ is the relativistic nucleon current operator of $cc1$ or $cc2$ forms as in ⁸. As bound state wave function we use Dirac-Hartree solutions from relativistic Lagrangians with scalar and vector meson terms ⁹. The wave function for the outgoing proton with asymptotic momentum \vec{p}_F is a solution

of the Dirac equation containing S-V global optical potentials¹⁰. In contrast to DWIA, in RDWIA the only fitted parameter is the spectroscopic factor^{5,6}. These RDWIA spectroscopic factors are larger than the DWIA ones⁶ and are valid both for low- and high- p_m data⁷.

We have recently studied^{11,12} the effect on the individual response functions of the relativistic treatment of the nucleon current. Within the relativistic plane wave impulse approximation (RPWIA) we showed¹¹ that the TL response is very sensitive to the negative-energy components of the relativistic bound nucleon wave function. We have also shown¹² that, for the $j = l \pm 1/2$ spin-orbit partners of a given shell, this sensitivity is much larger for the $j = l - 1/2$ than for the $j = l + 1/2$ case.

A certain degree of controversy surrounds the TL response measured in exclusive quasielastic electron scattering from the least bound protons in several nuclei (^{12}C , ^{16}O , ^{208}Pb): in some cases¹³ large deviations from standard DWIA calculations appear, while in others⁴ the data are close to the calculations. New data on the R_{TL} response for proton knockout from the $1p_{1/2}$ and $1p_{3/2}$ orbits of ^{16}O are available from Jefferson Laboratory (TJNAF) experiment 89-003¹⁴ at $|Q^2| \cong 0.8 (\text{GeV}/c)^2$. The purpose of this work is to show that there are important kinematical and dynamical relativistic effects for this case.

We can divide the differences between this fully relativistic approach and the standard nonrelativistic one into two categories: *i*) Effects due to the fully relativistic 4-vector current operator, compared to the nonrelativistic current operator which involves \vec{p}/M expansions. We call these effects *kinematical* as they are independent of the dynamics introduced by the nuclear interaction. *ii*) Effects due to the differences between relativistic and nonrelativistic nucleon wave functions, which depend on the 4-spinor structure and importantly on the potentials used in the respective Dirac and Schrödinger equations. We call these effects *dynamical*.

One may identify two types of relativistic dynamical effects: *ii - a*) Effects coming from the difference between the upper components of ψ_F (ψ_B) and the solutions χ_F (χ_B) of the Schrödinger equation. Assuming equivalent central and spin-orbit potentials, this difference stems from the well-known Darwin term. The influence of this term on $(e, e'p)$ observables has been demonstrated in several works^{6,15}. It appears to be the main dynamical relativistic effect in the cross section in the low- p_m region⁶, and is important for the correct determination of the spectroscopic factor from low- p_m data. Its omission reduces the spectroscopic factor by 15–20%. It is included in all calculations presented here. *ii - b*) The other dynamical effect is due to the negative-energy components of the relativistic ψ_B , ψ_F wave functions. Starting from Schrödinger-like solutions χ one may at best construct properly normalized four-spinors of the form

$$\psi = \frac{1}{\sqrt{N}} \left(\chi(\vec{p}), \frac{\vec{\sigma} \cdot \vec{p}}{E + M} \chi(\vec{p}) \right) \quad (2)$$

to calculate the relativistic nucleon current. However, this spinor lacks the dynamical enhancement of the lower component of the Dirac solution due to the relativistic S-V potentials. This dynamical enhancement is contained in the negative-energy components of the relativistic ψ_B (ψ_F) solutions and influences ($e, e'p$) observables in the high- p_m regions ¹¹.

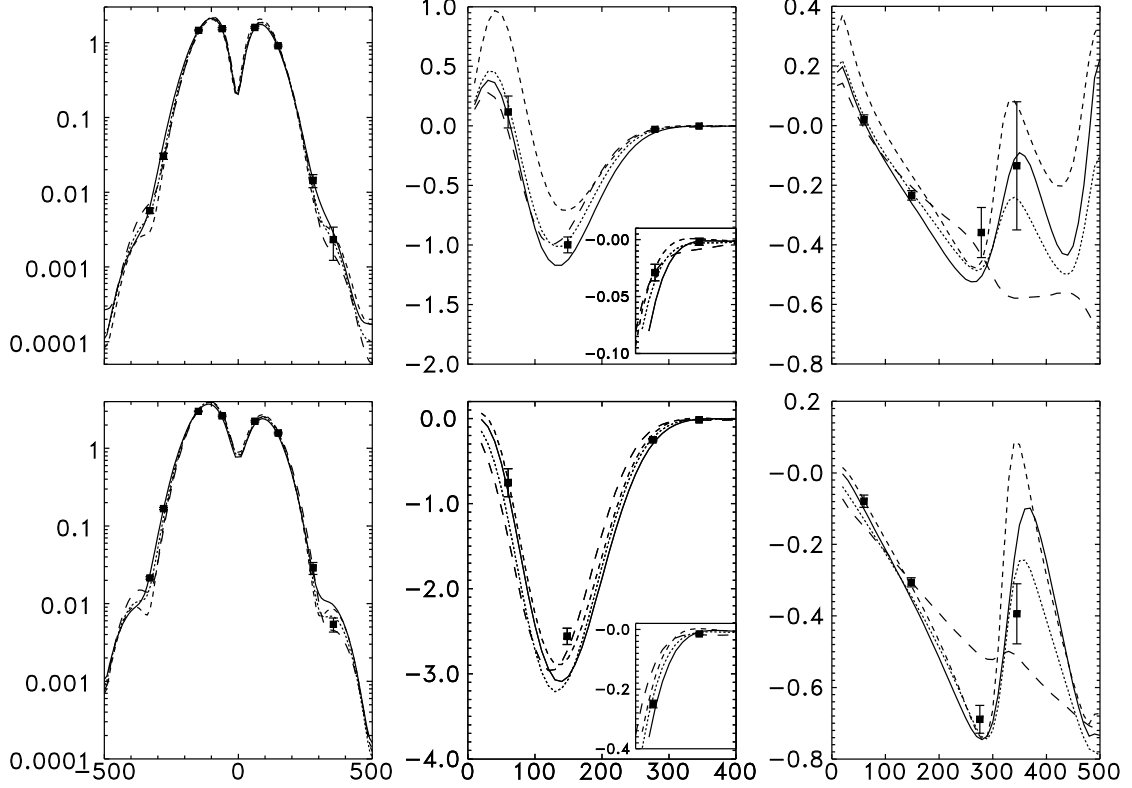


Fig. 1. Cross section in nb/(MeV sr) (left), R_{TL} in fm^3 (middle) and A_{TL} (right) for proton knockout from ^{16}O for the $1p_{1/2}$ (upper panel) and $1p_{3/2}$ (lower panel) orbits, versus missing momentum p_m in MeV/c. Results shown correspond to a fully relativistic calculation using the Coulomb gauge and the current operators: $cc1$ (solid line) and $cc2$ (dotted line). Also shown are the results after projecting the bound and scattered proton wave functions over positive-energy states (J_{++} , dashed line) and using the asymptotic momenta (J_{as} , long-dashed line). For the $p_{3/2}$ shell a small contribution was taken into account from the nearby $5/2^+$ and $1/2^+$ states known from the low- p_m data.

Fig. 1 shows the differential cross section, R_{TL} response and TL asymmetry (A_{TL}) for $p_{1/2}$ (top panels) and $p_{3/2}$ (bottom panels). R_{TL} and A_{TL} are obtained from the cross sections measured at $\phi_F = 0^\circ$ and $\phi_F = 180^\circ$ with the other variables (ω, Q^2, E_m, p_m) held constant, where ϕ_F is the azimuthal angle of the scattered proton (we follow the same convention as in ¹⁴). Relativistic calculations using the $cc1$ and $cc2$ current operators are shown by solid and dotted lines, respectively.

The Coulomb gauge has been used throughout this work. The role of the negative-energy components can be seen in Fig. 1 comparing the solid with the short-dashed lines. The dashed lines show the results obtained with the *cc1* current operator when the negative-energy components are projected out. We call J_{++}^μ the corresponding nucleon current, because ψ_F, ψ_B wave functions in eq. (1) are replaced by their positive energy projections ¹¹ $\psi_F^{(+)}, \psi_B^{(+)}$, respectively. The difference between the solid and short dashed lines is due to the dynamical enhancement of the lower components. It is important to realize that the positive-energy projectors needed to compute J_{++}^μ depend on the integration variable \vec{p} . One may attempt to neglect this dependence by using projection operators corresponding to asymptotic values of the momenta, *i.e.* projectors acting on ψ_F and ψ_B respectively, with $P_F^\mu = (E_F, \vec{p}_F), P_F^\mu - \bar{Q}^\mu$ the asymptotic four-momentum of the outgoing and bound nucleon respectively. We refer to this approach as *asymptotic projection* (J_{as}). The results corresponding to this approximation are shown by long dashed lines in Fig. 1. They are obtained with the *cc1* operator and are very similar for *cc2*.

Table 1. Spectroscopic factors obtained with the fully relativistic currents using *cc1* and *cc2* operators (second and third column), results obtained with the J_{++} and with J_{as} currents (see text) are presented in the fourth and fifth columns. For the $p_{3/2}$ shell we took into account the small contribution from the near lying $5/2^+$ and $1/2^+$ states known from the low- p_m data.

Shell	CC1	CC2	++ Proj.	As. Proj.
$1p_{1/2}$	0.72	0.77	0.83	0.77
$1p_{3/2}$	0.70	0.76	0.84	0.77

In Table 1 we show the spectroscopic factors needed by the different approximations. The spectroscopic factor simply scales down the curves for differential cross sections and R_{TL} while leaving A_{TL} unchanged. As seen in the left panel of Fig. 1, with these spectroscopic factors, the differential cross sections for $|p_m| < 300$ MeV/c are similar in the different approximations, but differ for $|p_m| > 300$ MeV/c where there is a substantial influence of negative energy components. Note that the two fully relativistic calculations, J_{cc1} (solid line) and J_{cc2} (dotted line), fit better the high- p_m data than the projected calculations. Note also that the cross sections obtained with positive-energy projected wave functions are more symmetrical around $p_m = 0$ than the RDWIA results. Therefore, the effect of removing the negative-energy components shows up more in R_{TL} and A_{TL} (see middle and right-hand panels of Fig. 1). Note that the dependence on the dynamical enhancement of the lower components is stronger for the $p_{1/2}$ R_{TL} response than for the $p_{3/2}$, a feature that was first seen in RPWIA ¹¹ and that persists in RDWIA. The agreement with experimental R_{TL} data is generally better for the fully relativistic calculations, even in the high- p_m region where data are more precise, and for the

$p_{1/2}$ shell where relativistic effects are more important. Particularly interesting is the oscillatory structure of the fully relativistic result for A_{TL} . This characteristic is preserved by the exact positive-energy projection method J_{++} , but not by J_{as} that severely modifies A_{TL} for both orbitals. We notice that the A_{TL} calculated with J_{as} are very similar to the ones obtained in ¹⁶, as the J_{as} calculation is similar to the EMA (noSV) of said reference. At low momentum this approach lies close to the fully relativistic ones and to the J_{++} ones, but beyond $p_m \simeq 200$ MeV/c they are noticeable different. The oscillating trend of the A_{TL} calculated in RDWIA is confirmed by the data ¹⁴ and agrees qualitatively with previous calculations by Van Orden ¹⁴. As it was the case for R_{TL} , the negative energy components clearly affect the A_{TL} of the $j = l - 1/2$ partner, largely improving the agreement with experiment. The experimental error bars for this observable at high- p_m should be reduced by a factor two or more to have more conclusive evidence. Anyway, for the $p_{3/2}$ shell the asymptotic calculation clearly fails to reproduced the experimental data, except for the point at around 150 MeV, where all the calculations predict very similar results.

Other relativistic effects can be seen in Fig. 2, where we compare RDWIA results on A_{TL} (left panels) and R_{TL} (right panels) to nonrelativistic approaches at various levels. To minimize the differences we have used the $cc2$ current operator and nonrelativistic scattered wave functions obtained from Dirac-equivalent Schrödinger equations. This ensures that the nonrelativistic wave functions correspond to the upper components of the relativistic ones, containing in particular the Darwin term. For the nonrelativistic bound wave functions, we used the ones in ¹⁷. In said reference new approximations to the on-shell relativistic one-body current operator were developed to take better account of relativistic kinematic effects in nonrelativistic calculations. In particular, the charge density contains a spin-orbit correction that affects R_{TL} ¹⁷. In Fig. 2 we show by long dashed lines the results obtained with the “relativized current” and by dotted lines the results obtained with that relativized current when the spin-orbit correction term to the charge-density is neglected. One can see that the spin-orbit correction has a very large effect on R_{TL} and A_{TL} . Its omission causes large deviations from the relativized current results. Using the DWEEPY ¹⁸ code we have obtained for A_{TL} similar results to the dotted lines in Fig. 2.

The short dashed lines in Fig. 2 are results obtained with the relativistic current and 4-spinors constructed as in eq. (2) from the nonrelativistic bound and scattered wave functions. In this way, the relativistic kinematic is fully taken into account, only the dynamical enhancement of the lower components is missed. This is why these results (short-dashed lines) for A_{TL} and R_{TL} are much closer to the fully relativistic results shown by the solid lines. We see also that a large oscillation of A_{TL} can be recovered in the nonrelativistic approach. The much smaller oscillation of A_{TL} is a distinctive feature of the J_{as} results, and it seems to be ruled out by the

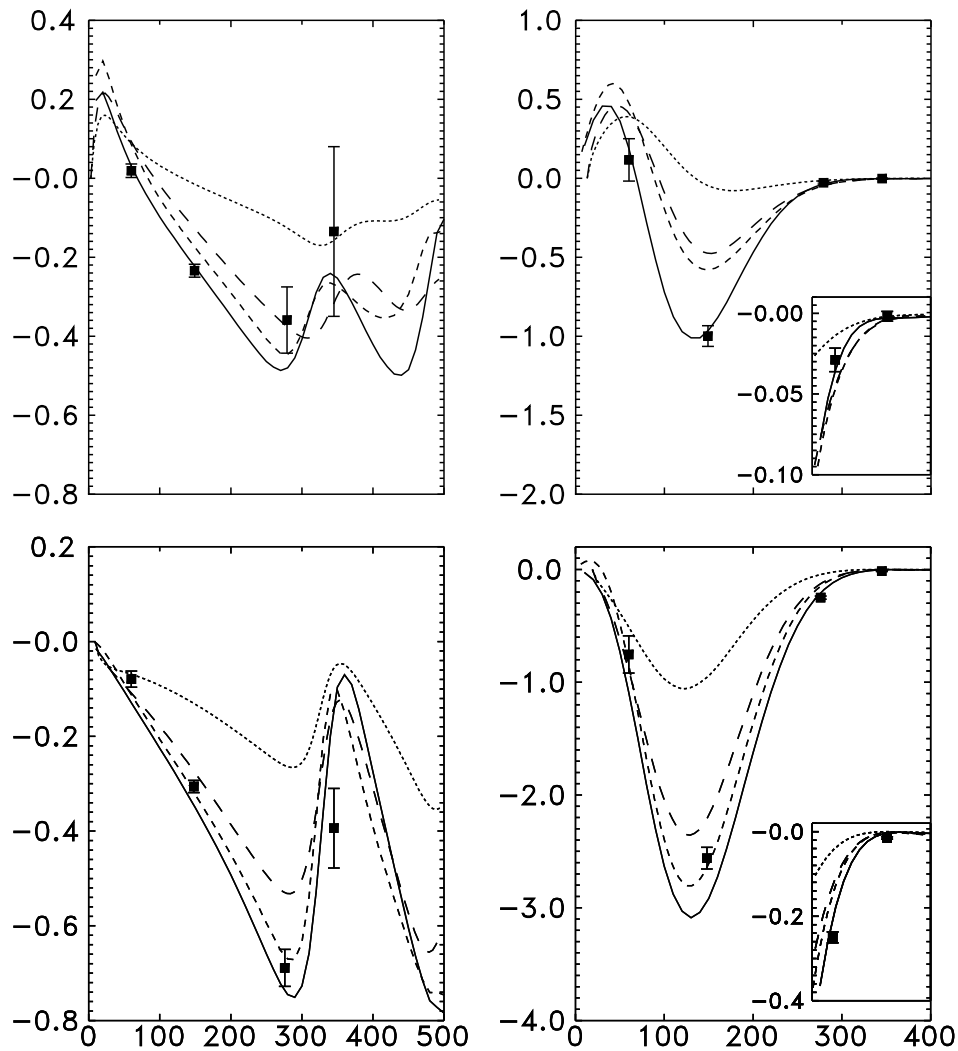


Fig. 2. R_{TL} (right panels) and A_{TL} asymmetries (left panels) for proton knockout from ^{16}O for the $1p_{1/2}$ (top panels) and $1p_{3/2}$ (bottom panels) orbits. Results shown correspond to a fully relativistic calculation using the Coulomb gauge and the current operator $cc2$ (solid line), a calculation performed by projecting the bound and scattered proton wave functions over positive-energy states (dashed line) and two nonrelativistic calculations with (long-dashed) and without (dotted) the spin-orbit correction term in the charge density operator (see text for details).

experiment. We also note that, while the effect of the dynamical enhancement of the lower components is larger in $p_{1/2}$ than in $p_{3/2}$ shells, the effects of relativistic kinematics are of the same order in both shells. Everything put together, the data on A_{TL} and R_{TL} are a strong indication of the presence and crucial role played by dynamical effects of relativity affecting the lower components, in the description of electron-nucleus scattering reactions.

In conclusion, we have identified two types of relativistic effects on R_{TL} and A_{TL} . One is of kinematical origin, and has a large contribution from the spin-orbit correction to the charge density, and other is of dynamical origin. The latter is mainly due to the enhancement of the lower components and is stronger for $p_{1/2}$ than for the $p_{3/2}$ orbital. This is in addition to the dynamical effect on the upper component due to the Darwin term which is present in all the results given here, and that mostly affects the determination of spectroscopic factors ⁶. It is encouraging that the data ¹⁴ agree so well with the predictions of the fully relativistic calculations and one anticipates being able to make even more stringent tests when a finer grid of high-precision data involving other nuclei become available in the range $200 \leq p_m \leq 400$ MeV/c.

Acknowledgments

This work was partially supported under Contracts No. 940183 (NATO Collaborative Research grant), #DE-FC01-94ER40818 (cooperative agreement with the US department of Energy D.O.E.), PB/95-0123, PB/95-0533-A, PB/95-1204 (DG-ICYT, Spain), PB/96-0604 (DGES, Spain), PR156/97 (Complutense University, Spain) and by the Junta de Andalucía (Spain).

References

1. S. Boffi, C. Giusti, F. Pacati, M. Radici in “*Electromagnetic Response of Atomic Nuclei*”, (Oxford-Clarendon Press, 1996), and refs. therein
2. I. Bobeldijk et al., Phys. Rev. Lett. **73** (1994) 2684
3. H. Müther, W.H. Dickhoff, Phys. Rev. **C49** (1994) R17
4. L. Chinitz *et al.*, Phys. Rev. Lett. **67** (1991) 568
5. A. Picklesimer, J.W. Van Orden, Phys. Rev. **C35** (1987) 266; *ibidem* **C40** (1989) 290
6. J.M. Udías *et al.*, Phys. Rev. **C48** (1993) 2731; **C51** (1995) 3246
7. J.M. Udías, P. Sarriguren, E. Moya de Guerra, J.A. Caballero, Phys. Rev. **C51** (1996) R1488
8. T. de Forest, Nucl. Phys. **A392** (1983) 232
9. B.D. Serot, J.D. Walecka, Adv. Nucl. Phys. **16** (1986) 1
10. E.D. Cooper, S. Hama, B.C. Clark, R.L. Mercer, Phys. Rev. **C47** (1993) 297
11. J.A. Caballero, T.W. Donnelly, E. Moya de Guerra, J.M. Udías, Nucl. Phys. **A632** (1998) 323
12. J.A. Caballero, T.W. Donnelly, E. Moya de Guerra, J.M. Udías, Nucl. Phys. **A643** (1998) 189
13. G.M. Spaltro *et al.*, Phys. Rev. **C48** (1993) 2385. H.J. Bulten, Ph.D. thesis, University of Utrecht, 1992

14. T Saha *et al.* TJNAF proposal 89-003 (1989). J. Gao, Ph.D. Thesis, MIT (1999)
15. S. Boffi, C. Giusti, F.D. Pacati, F. Cannata, Nuovo Cimento **98**, (1987) 291; Y. Jin, D.S. Onley, Phys. Rev. **C50** (1994), 377
16. J.J. Kelly, Phys. Rev. **C56** (1997) 2672; nucl-th/9905024
17. J.E. Amaro *et al.*, Nucl. Phys. **A602** (1996) 263; *ibid.* **A611** (1996) 163
18. C. Giusti, F. Pacati, Nucl. Phys. **A473** (1987) 717; **A336** (1980) 427